Available online at www.sciencedirect.com
ScienceDirect
International Journal of Heat and Mass Transfer 50 (2007) 1683–1693
International Journal of HEAT and MASS TRANSFER
www.elsevier.com/locate/ijhmt

Numerical investigation of turbulent natural convection in an inclined square cavity with a hot wavy wall

M. Aounallah [a,*], Y. Addad [b], S. Benhamadouche [b,c], O. Imine [a], L. Adjlout [a], D. Laurence [b,c]

[a] Department of Marine Engineering, Faculty of Mechanics, P.O. Box 1505, El-Mnaouar, Algeria
[b] School of Mechanical, Aerospace and Civil Engineering, The University of Manchester, P.O. Box 88, Sackville Street, Manchester M60 1QD, UK
[c] Electricité de France R&D, Département de Mécanique des Fluides et Transferts Thermiques (MFTT), 6 Quai Watier, 78400 Chatou, France

Received 18 October 2005; received in revised form 16 October 2006
Available online 13 December 2006

Abstract

The turbulent natural convection of air flow in a confined cavity with two differentially heated side walls is investigated numerically up to Rayleigh number of 10^{12}. The objective of the present work is to study the effect of the inclination angle and the amplitude of the undulation on turbulent heat transfer. The low-Reynolds-number k–ε, k–ω, k–ω–SST RANS models and a coarse DNS are used and compared to the experimental benchmark data of Ampofo and Karayiannis [F. Ampofo, T.G. Karayiannis, Experimental benchmark data for turbulent natural convection in an air filled square cavity, Int. J. Heat Mass Transfer 46 (2003) 3551–3572]. The k–ω–SST model is then used for the following test-cases as it gives the closest results to experimental data and coarse DNS for this case. The mean flow quantities and temperature field show good agreement with coarse DNS and measurements, but there are some slight discrepancies in the prediction of the turbulent statistics. Also, the numerical results of the heat flux at the hot wall are over predicted. The strong influence of the undulation of the cavity and its orientation is well shown. The trend of the local heat transfer is wavy with different frequencies for each undulation. The turbulence causes an increase in the convective heat transfer on the wavy wall surface compared to the square cavity for high Rayleigh numbers. A correlation of the mean Nusselt number function of the Rayleigh number is also proposed for the range of Rayleigh numbers of 10^9–10^{12}.

Keywords: Natural convection; Undulation; k–ω–SST model; Coarse DNS; Heat transfer

1. Introduction

Turbulent natural convection in cavities with two differentially heated side walls enjoys noticeable interest from the thermal sciences communities. The importance of this case is due to the fact that natural convection in enclosures can be found in many industrial or civil engineering applications such as energy transfer in rooms and buildings, nuclear reactor cooling, solar collectors and electronic component cooling. A significant number of experimental and theoretical works have been carried out in the past decades in an attempt to understand turbulent flow in enclosures. Comprehensive reviews of turbulent natural convection has been documented in the literature; see e.g. Markatos and Pericleous [2], Kuyper et al. [3], Janssen et al. [4] and Said et al. [5]. However, predictions of turbulent buoyant flows have been successful for only limited cases due to the difficulty of the numerical simulation of boundary layers near the walls and the uncertainly of the general turbulence models for turbulent natural convection. The flow in turbulent natural convection in a square cavity is characterised by a thin boundary layer along the walls while the core is thermally stratified. The flow gradients are very large in the boundary layer and require a large number of grid points. Previous work has shown that the low-Reynolds approach can be adequately applied to calculate turbulent natural convection in opposition with computations using high Reynolds averaged Navier–Stokes

* Corresponding author. Tel.: +00 213 4158 4323; fax: +00 213 4158 4354.
E-mail address: aounalah@univ-usto.dz (M. Aounallah).

0017-9310/$ - see front matter © 2006 Elsevier Ltd. All rights reserved.
doi:10.1016/j.ijheatmasstransfer.2006.10.015

Nomenclature

a	thermal diffusivity
b	amplitude of the wavy wall
g	gravitational acceleration
H	cavity width
k	turbulent kinetic energy
Nu_l	local Nusselt number, $-(\partial T/\partial x)_w H/\Delta T$
Nu_a	average Nusselt number, $1/H \int_0^1 Nu\,dy$
P	pressure
Pr	Prandtl number, v/a
Ra	Rayleigh number, $g\beta\Delta T H^3/av$
T	temperature
T_0	reference temperature, $(T_h + T_c)/2$
t'	temperature fluctuation
U_i	mean velocity components in the ith direction
u_i'	fluctuating velocities in the ith direction
V_0	reference velocity, $\sqrt{g\beta\Delta TH}$
x_i	Cartesian space coordinate ($i = 1, 3$)

Greek symbols

β	thermal expansion coefficient
ΔT	temperature differences, $(T_h - T_c)$
ε	dissipation rate of k
μ	dynamic viscosity
ρ	fluid density
σ_k, σ_ω	model constants
ω	turbulent frequency

Subscripts

c, h	cold, hot wall
t	turbulent

models where, the solution of the boundary layer is assumed using the so called "universal" logarithmic profile.

Although developing advanced wall functions adapted to natural convection has been recently attempted [6], conventional literature shows that the equations must be solved up to the wall for calculating the boundary layers in turbulent natural convection due to the boundary layer thickening/thinning along the walls. One of the most popular turbulence models for a correct treatment of the flow up to the wall are the low-Reynolds-number (LRN) k–ε models. Henkes et al. [7] calculated turbulent natural convection using different low-Reynolds-number k–ε models in a square cavity. Three different turbulence models were compared: the standard k–ε model with logarithmic wall functions, the low-Reynolds-number model of Chien [8] and the model of Jones and Launder. Comparisons of the averaged wall-heat transfer with experiments for tall vertical cavities show that the standard k–ε model gives a 30% over prediction.

Dol and Hanjalić [9] carried out a computational study of turbulent natural convection in a side-heated near-cubic enclosure at a Rayleigh of 4.9×10^{10} using the RANS approaches. Their computations were performed with both two-dimensional and three-dimensional codes using the low-Reynolds-number k–ε model (KEM) of Chien and advanced second-moment closures (SMC). They showed that SMC is better in capturing thermal 3D effects and strong streamlines curvature at the corners. Peng and Davidson [10] investigated the performance of the low-Reynolds-number k–ω model on the turbulent buoyant convection flows with thermal stratification. The authors reported a problem commonly encountered at moderate Rayleigh numbers ($Ra = 10^{10}$–10^{12}): when applying the k–ε model to buoyancy-driven cavity flows, the model is not capable of returning grid-independent predictions owing to the transition regime along the vertical walls. It was found that the buoyancy source term of the turbulence kinetic energy, G_k, exhibits strong grid sensitivity, as this term is modelled with the Standard gradient diffusion hypothesis (SGDH). By introducing a damping function, the above grid dependence problem is eliminated. Furthermore, the modified G_k renders a correct asymptotic behaviour near the vertical wall. Hsieh and Lien [11] investigated numerically the buoyancy-driven turbulent flows in enclosures similar to those used by Betts and Bokhari [12] and Tian and Karayiannis [13,14] using variants of Lien and Leschziner's (LL) model and the two layer approach. In the case of the tall cavity, the performance of the LL model in terms of mean velocity and temperature profiles are found generally fairly well compared to the experimental data.

In addition to RANS modelling, as computing resources are constantly growing fine techniques such as DNS, coarse DNS and LES has attracted great attention and have been increasingly implemented in commercial and industrial CFD codes. Various sub-grid scale (SGS) models have been used in LES and shown encouraging performance, in which the study and comparison have usually been subjected to the well known Rayleigh–Bénard convection, for example: the simulation of Pallares et al. [15] on a perfectly conducting cubic cavity. Peng and Davidson [16] studied the turbulent buoyant flow in a cavity using LES technique and found their simulation able to reasonably reproduce the global mean flow and thermal field in a satisfactory agreement with the experiment. Boudjemadi et al. [17] used DNS to produce full budgets of Reynolds stresses and heat fluxes for an infinitely tall cavity at Rayleigh numbers similar to the Betts and Bokhari [12] cavity. These were soon complemented by Versteegh and Nieuwstadt [18]. Both papers show intricate coupling, via gravity, between dynamic and thermal second moments. Dol et al. [19] presented some results of the computation of natural convection in the tall cavity, obtained with a fully differential and

a four-equation ($k-\varepsilon-\overline{\theta^2}-\varepsilon_{\theta\theta}$) algebraic model. Despite the unsatisfactory reproduction of individual terms in the equations, computations yielded acceptable agreement with available experimental and DNS data.

Kenjereš et al. [20] studied the natural convection in an air-filled cubical cavity under different angles of inclinations. Salat et al. [21] conducted an experimental and numerical investigation of turbulent natural convection in a large air-filled cavity. The numerical approximation was achieved with three different approaches. The first is by directly solving the unsteady three-dimensional Navier–Stokes equations (DNS). The second is by filtering the equation in time and modelling the Reynolds stress (RANS). Finally, by filtering the equation in space and modelling the sub-grid dynamic stress and heat flux (LES). In the experiment, temperature is measured by micro thermocouples and velocity by Laser Doppler Anemometer (LDA). The authors compared both mean flow quantities, temperature and turbulence statistics of the numerical simulations with the experimental measurements. An advanced turbulence model for buoyancy-driven flows has been developed and validated by Liu and Wen [22]. Kenjereš et al. [23] present a recent development in modelling and numerical computations of natural and mixed convection based on newly developed-nonlinear algebraic heat flux and buoyancy extended stress models in the framework of the eddy-viscosity with the elliptic-relaxation approach. For all the simulations, good agreement with available experimental results and earlier numerical simulations is obtained.

The experiment of Betts and Bokhari [12] has been undertaken to investigate the turbulent natural convection of air in a tall differentially heated rectangular cavity at a low Rayleigh number. The aim of their work was to measure the mean and turbulent quantities for velocity and temperature within the cavity. Tian and Karayiannis [13,14] presented the thermal and the fluid flow fields and the turbulence quantities for a low turbulent natural convection in an air-filled square cavity. Temperature and velocity distribution were symmetrically and simultaneously measured at different locations in the enclosure. They found that temperature and velocity fluctuations were limited in the boundary layers along the solid walls and did not have a Gaussian distribution. Recently, Ampofo and Karayiannis [1] presented an experimental benchmark data for turbulent natural convection in an air-filled square cavity usable for validation of CFD codes.

The aim of this paper is to examine different RANS models in predicting the flow in the square cavity and compare the results with the experimental data of Ampofo and Karayiannis [1] and the coarse DNS data. The second objective is to use the RANS model that is more suited to this type of flows to study the effect of turbulence on natural convection in a cavity with a wavy wall. The present work is a continuation of the work of Adjlout et al. [24] concerning the influence of the inclination angle on the local and the average Nusselt numbers across a square undulated cavity in the laminar regime. In their study it was reported that the mean Nusselt number decreases in comparison to the square cavity with smooth walls. Here, the low-Reynolds-number k–ε, k–ω, k–ω–SST models are tested and comparison is made with the coarse DNS predictions and experimental benchmark data of Ampofo and Karayiannis [1]. The finite volume method is used to discretize the partial differential equations. Grid independence is carried out with the k–ω–SST model for the undulated cavity when no experimental data are available in this case. The present study intends to focus on the influence of the inclination angle and the amplitude of the undulation on the local Nusselt number for various Rayleigh numbers up to 10^{12}. This is of great interest in the industrial applications mentioned above, as it will give a better understanding of the undulations advantages over the smooth walls.

2. Problem position

The problem treated is statistically a two-dimensional heat transfer in an inclined square cavity. The hot wall is wavy with a constant temperature T_h. The opposite wall is cold with a constant temperature T_c while the horizontal walls are insulated. Fig. 1 shows the geometry of the cavity under consideration and the coordinates chosen. The cavity is filled with air ($Pr = 0.71$) and the Rayleigh number is varied up to 10^{12}.

3. Mathematical formulation

The turbulent viscous flow inside a confined enclosure and the temperature distribution are described by the steady Navier–Stokes, the energy and turbulent equations. The Boussinesq approximation is used. The governing

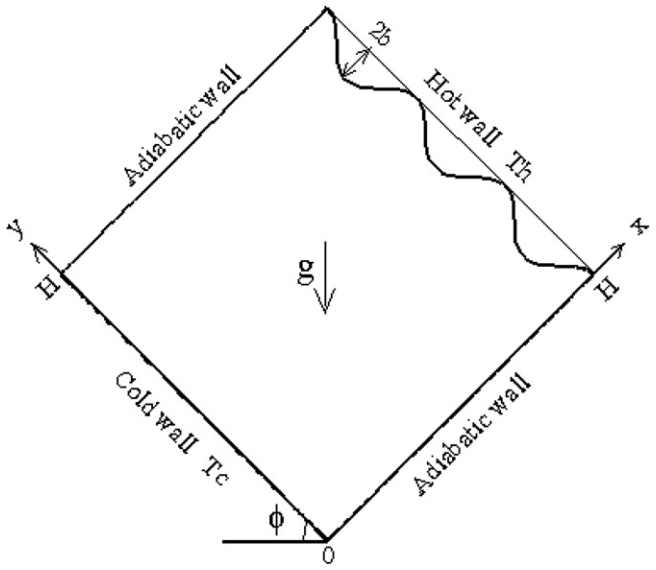

Fig. 1. Computational domain.

equations associated with the k–ω–SST [25] model are defined as follow:

$$\frac{\partial(\rho U_i)}{\partial x_i}=0 \tag{1}$$

$$\frac{\partial(\rho U_j U_i)}{\partial x_j}=-\frac{\partial p}{\partial x_i}+\frac{\partial}{\partial x_j}(\mu+\mu_t)\left(\frac{\partial U_i}{\partial x_j}+\frac{\partial U_j}{\partial x_i}\right)+g_i\rho\beta(T-T_0) \tag{2}$$

$$\frac{\partial(\rho U_j T)}{\partial x_j}=\frac{\partial}{\partial x_j}\left[\left(\rho a+\frac{\mu_t}{Pr_t}\right)\frac{\partial T}{\partial x_j}\right] \tag{3}$$

$$\frac{\partial(\rho U_j k)}{\partial x_j}=\frac{\partial}{\partial x_j}\left[\left(\mu+\frac{\mu_t}{\sigma_k}\right)\frac{\partial k}{\partial x_j}\right]+\tilde{\tilde{P}}_k-\beta^*\rho k\omega+G_k \tag{4}$$

$$\frac{\partial(\rho U_j \omega)}{\partial x_j}=\frac{\gamma}{\alpha_t}P_k-\beta\rho\omega^2+\frac{\partial}{\partial x_j}\left(\mu+\frac{\mu_t}{\sigma_\omega}\right)\frac{\partial\omega}{\partial x_j}+(1-F_1)2\rho\sigma_{\omega 2}\frac{1}{\omega}\frac{\partial k}{\partial x_j}\frac{\partial\omega}{\partial x_j} \tag{5}$$

$$\text{with}\quad G_k=-g_j\rho\beta\frac{\Delta T}{Pr_t}\frac{\partial T}{\partial x_j} \tag{6}$$

$$P_k=\mu_t\left(\frac{\partial U_i}{\partial x_j}+\frac{\partial U_j}{\partial x_i}\right)\frac{\partial U_i}{\partial x_j} \tag{7}$$

$$\tilde{\tilde{P}}_k=\min(P_k, C_1\varepsilon),\quad C_1=10 \tag{8}$$

$$\alpha_t=\frac{k}{\omega}$$

For the SST model of Menter [25], the coefficients are expressed in the following form:

$$C_\phi=F_1C_{\phi 1}+(1-F_1)C_{\phi 2} \tag{9}$$

where C_ϕ stands for any constant in the two differential equations. The blending function F_1 that goes from one near the surface to zero away from the wall is given by

$$F_1=\tanh\left(\arg_1^4\right) \tag{10}$$

where

$$\arg_1=\min\left[\max\left[\frac{\sqrt{k}}{0.09\omega y};\frac{500y}{y^2\omega}\right];\frac{4\rho k}{\sigma_{\omega 2}CD_{k\omega}y^2}\right] \tag{11}$$

$$CD_{k\omega}=\max\left[\frac{2\rho}{\omega\sigma_{\omega 2}}\frac{\partial k}{\partial x_j}\frac{\partial\omega}{\partial x_j};10^{-20}\right] \tag{12}$$

The coefficients set 1 are

$$\sigma_{k1}=1.176,\quad \sigma_{\omega 1}=2,\quad \beta_1=0.075,\quad \beta_1^*=0.09,$$

$$\alpha_1=\frac{\beta_1}{\beta_1^*}-\frac{1}{\sigma_{\omega 1}}\frac{k^2}{\sqrt{\beta_1^*}},\quad k=0.41$$

and the coefficients set 2 are

$$\sigma_{k2}=1,\quad \sigma_{\omega 2}=1.168,\quad \beta_2=0.0828,\quad \beta_2^*=0.09,$$

$$\alpha_2=\frac{\beta_2}{\beta_2^*}-\frac{1}{\sigma_{\omega 2}}\frac{k^2}{\sqrt{\beta_2^*}}$$

$$S_\omega=2(1-F_1)\frac{1}{\sigma_{\omega 2}}\frac{1}{\omega}\frac{\partial k}{\partial x_j}\frac{\partial\omega}{\partial x_j} \tag{13}$$

The eddy-viscosity for this model is

$$\mu_t=\rho\frac{a_1k}{\max(a_1\omega;\Omega^*F_2)} \tag{14}$$

where $a_1=0.31$

$$F_2=\tanh\left(\arg_2^4\right) \tag{15}$$

$$\arg_2=\max\left[2\frac{\sqrt{k}}{0.09\omega y};\frac{500y}{y^2\omega}\right] \tag{16}$$

$$\Omega^*=\sqrt{\frac{1}{2}\Omega_{ij}\Omega_{ij}} \tag{17}$$

For the low-Reynolds-number models, ω at the near-wall cell is fixed algebraically according to

$$\omega_p=\frac{6v}{\beta_1y^2} \tag{18}$$

The undulation equation is expressed as follows:

$$f(y)=[1-b+b(\cos 2\pi ny)] \tag{19}$$

where n and b are respectively, the number of undulations and the amplitude.

4. Numerical procedure

The coupled conservation equation (1)–(5) are solved numerically using FLUENT 6.1.22 code for k–ω–SST model and *Saturne*® in-house EDF code is used for coarse DNS simulations. *Saturne* code has been successfully used for LES simulations both with the standard Smagorinsky model and the dynamic one (see [26, 27]). The first code uses a segregated solver and the finite volume method to discretize the above partial differential equations on a grid where all the variables are collocated. The second order upwind scheme is employed for the convection term in the momentum and energy equations, while, the convection term in the turbulence transport equations is discretized using the first order upwind scheme. The pressure–velocity coupling is ensured using the SIMPLE algorithm. The cavity is filled with a non-uniform rectangular grid with a very fine spacing near the walls, as needed for accurately resolving the steep gradients in the thin buoyancy-driven boundary layer. As is shown in Fig. 2, the 2D computational grids are staggered and clustered towards the walls. All the variables are calculated right up to the walls without using any wall function. On the wall surface, the boundary values for the velocity components and the turbulent kinetic energy are set to zero. The dimensionless temperature of the cold and the hot walls are 0 and 1 respectively. The residuals of continuity, momentum and energy equations are required to be below 10^{-6} in order to reach a fully converged solution. The relaxation parameters have been adjusted for each simulation in order to accelerate convergence. *Saturne* code uses a collocated unstructured finite volume technique to discretize the Navier–Stokes equations. The algorithm is based on a SIMPLEC algorithm for pressure–velocity coupling with a Rhie and Chow interpolation to avoid odd–even decoupling problem. The discretisation is second order in space thanks to a

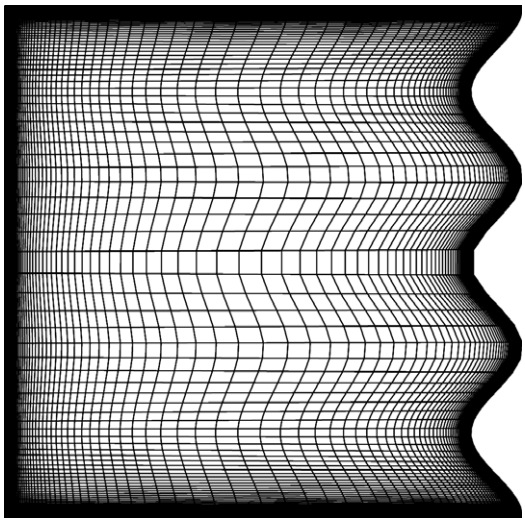

Fig. 2. Computational grids.

reconstruction technique for the gradients and second order in time using a Crank–Nicolson scheme (with Adams Bashforth extrapolation for the mass flow). A fully centred scheme is used in treating the velocity convection term while a slope test is employed for temperature to ensure a physical solution between the imposed limits (solution $T \in [T_c, T_h]$). For large eddy simulation both the standard Smagorinsky and the dynamic model based on Germano's identity are available. A coarse DNS is used herein (no sub-grid scale model is used) as the standard Smagorinsky did not give a satisfactory solution. This is not surprising as the flow is laminar in large parts of the domain and the standard Smagorinsky model is not suitable for transition. In addition the grid is well refined such as the computations switch to a quasi-DNS in a large portion of the domain.

5. Validation

Before considering the cavity with the undulated hot wall, the square case is tested under the same conditions of turbulence and compared to the 3D experimental benchmark data of Ampofo and Karayiannis [1]. These authors have conducted an experimental study of low-level turbulence natural convection in an air-filled vertical square cavity of 0.75 m high × 0.75 m wide × 1.5 m deep giving a 2D flow in the middle-plane. The hot and the cold walls were isothermal at 50 °C and 10 °C respectively, giving a Rayleigh number of 1.58×10^9. The local velocity and temperature were simultaneously measured at different locations in the cavity and both mean and *rms* quantities were presented. In the present study, a coarse DNS simulation is performed with *Saturne* code on a cubic cavity with $96 \times 96 \times 32$ cells grid. On the other hand, the computed turbulent buoyant flow with the low-Reynolds-number k–ε, k–ω and k–ω–SST models is carried out using FLUENT code.

In regard to the case at Rayleigh number of 1.58×10^9, the experimental results showed that the fluid pattern is basically laminar except close to the side walls. In order to compare experimental and numerical approaches in the median vertical plane, the profiles of the vertical velocity (a) and the temperature (b) are respectively displayed in Fig. 3. The buoyant velocity V_0 is used as a normalisation parameter for the velocity. Due to the symmetry of the profiles and stagnant fluid in the core of the box, only the closest part to the wall at mid height is presented to show more clearly the thin thermal boundary layers. As seen in Fig. 3, agreement between the coarse DNS and both k–ω models and the experimental data in terms of mean velocity and temperature profiles at $y/H = 0.5$ is fairly good. However, a large discrepancy between the k–ε model predictions and the measured values is observed. The peak velocity value is particularly well captured by all simulations except the k–ε model which largely over predicts the peak of the vertical velocity. The flow stratification is well observed in the most width of the cavity except where it merges with the wall plume. All simulations

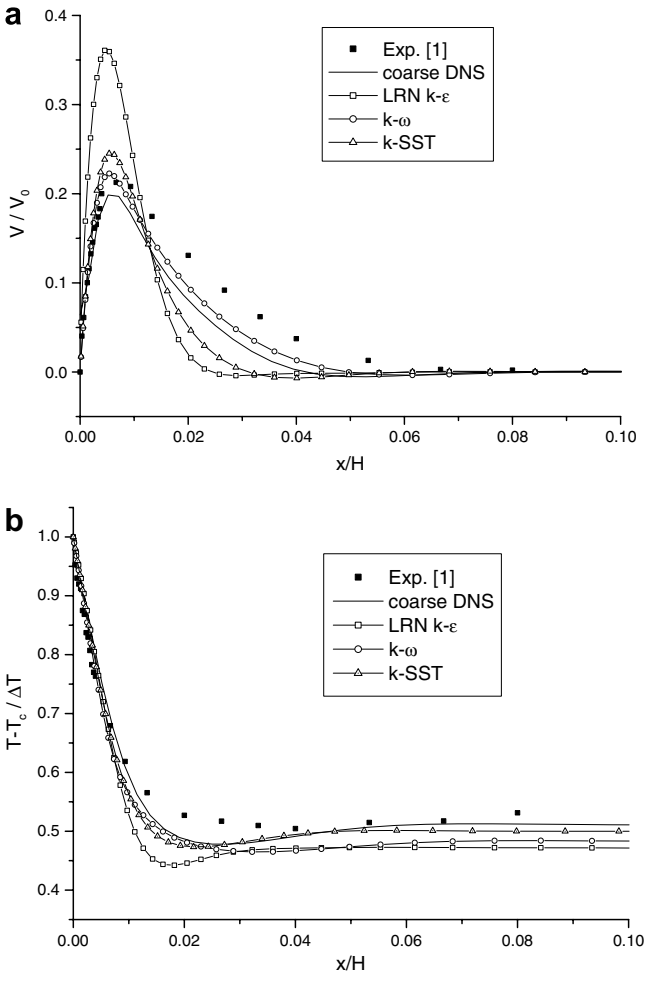

Fig. 3. Comparison of the vertical velocity (a) and the temperature (b) at $y/H = 0.5$ for the square cavity ($Ra = 1.58 \times 10^9$ and $\phi = 90°$).

seem to predict insufficient mixing between in the outer layer as the buoyant jet entrains stagnant fluid in the cavity. Compared to the experimental data, the k–ω model gives the best prediction of the velocity, while understandably the coarse DNS is the closest one for the temperature prediction. The k–ω–SST model is globally satisfactory despite some discrepancies concerning the vertical velocity component and the turbulent kinetic energy. In the enclosure core region there is very little activity: the mean temperature is nearly uniform, the fluid velocity is very small and so is the turbulence level, turbulent stresses and heat flux. The mean temperature shows high gradients in the wall boundary-layer with an almost uniform distribution in the enclosure core. The predicted temperatures all show minimum which is lower than the measured values in the core of the enclosure. This is a trace of the cold draft emanating from the opposite wall, which according to measurements should have had time to completely mix while crossing over along the floor. Again this indicates insufficient mixing with the laminar core and perhaps too early relaminarisation in the models. All the simulations return a temperature of 0.5 at the centre of the cavity, as required by symmetry, but this is not visible on the near wall profiles (Fig. 3).

Fig. 4 displays the measured turbulence kinetic energy on the mid-width plane and the corresponding profiles obtained with the numerical simulations. On one hand, the experimental profile is asymmetrically (not seen here) distributed between the hot and the cold walls, and reaches its maximum close to the walls. On the other hand, numerical prediction of turbulence kinetic energy is symmetric. Comparison indicates that all the numerical prediction induces lower turbulence kinetic energy especially both k–ω models. In the core, at the middle section, the turbulent kinetic energy falls to zero.

Fig. 5 shows the heat transfer rate along the hot wall expressed in terms of the local Nusselt number distribution.

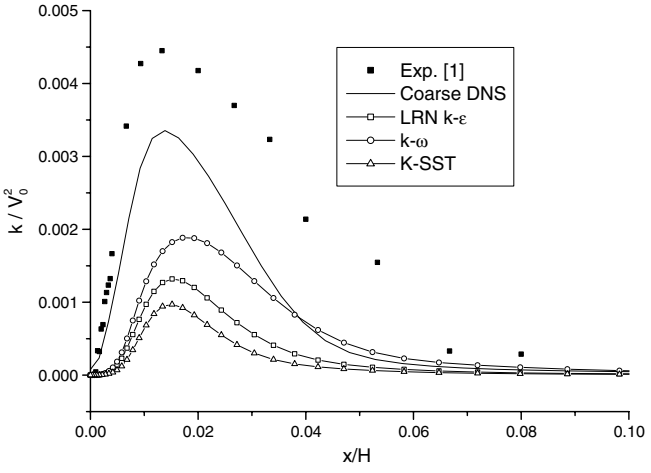

Fig. 4. Comparison of the turbulent kinetic energy at $y/H = 0.5$ for the square cavity ($Ra = 1.58 \times 10^9$ and $\phi = 90°$).

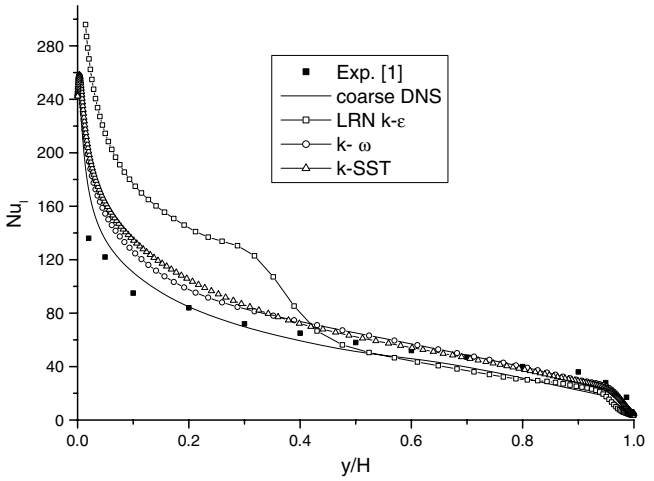

Fig. 5. Comparison of the local Nusselt number at the hot wall for the square cavity ($Ra = 1.58 \times 10^9$ and $\phi = 90°$).

The deficit of the k–ε model prediction is well observed in the first part along the wall. Qualitatively, the trend of the predicted profiles by the coarse DNS, then both k–ω models are in satisfactory agreement with experimental data. In general, both k–ω models and the coarse DNS over predict Nusselt number with 17.5% and 1.5% respectively, on the lower half of the wall then under-predict it but somewhat less strongly compared to the experiment. It should be noted that the Nusselt distribution displayed by k–ω model calculation, though better than using LRN k–ε, is still somewhat unsatisfactory in particular on the lower part. The Nusselt distributions predictions by k–ω and k–ω–SST are quite similar as shown in Fig. 3. Note, however, that the numerical simulations predict a greater value in the region near the hot and the cold walls. The loss may have affected the measured position of transition onset along the active walls. The overprediction of the Nusselt number in the initial part of the heated wall may related to the local minimum of temperature and residual cold draft coring over from the opposite wall, which induces the sharper temperature gradients seen in Fig. 3. The k–ω–SST performance is similar to the k–ω and will be retained for subsequent simulations as it has a rapid straining production limiter which can be beneficial along the wavy wall, Hutton et al. [28].

It is desirable to obtain an asymptotically grid-independent solution by means of refined grid. To determine the accuracy of the numerical solution, the grid-independent study using k–ω–SST model on grids of respectively 100×100, 120×120 and 200×200 cells is depicted in Figs. 6 and 7. As it can be seen, the three profiles are practically collapsing on one curve across the cavity, when the grids are refined. Virtually, there is no difference between the profiles, especially for the vertical velocity and the local Nusselt number. The only visible effect of grid refinement is on the temperature profile in the thin boundary layer which can be seen by a slight deviation. The curva-

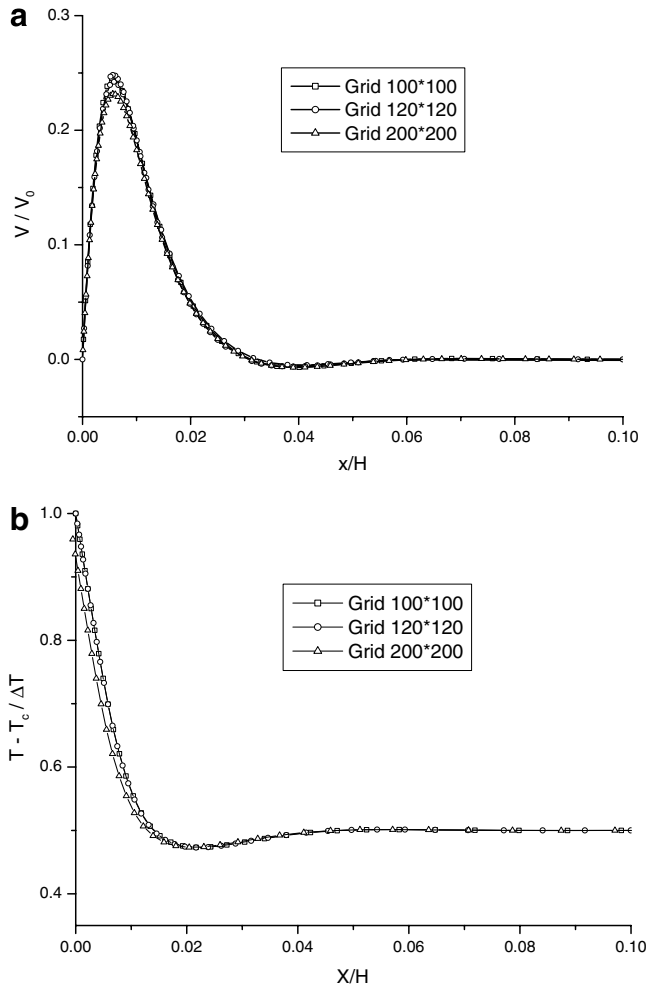

Fig. 6. Grid dependence tests of the solution: vertical velocity (a) and the temperature (b) at $y/H = 0.5$ for the square cavity ($Ra = 1.58 \times 10^9$ and $\phi = 90°$).

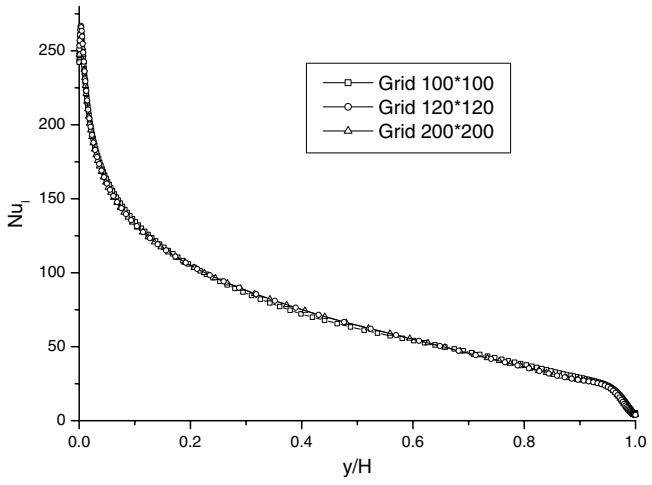

Fig. 7. Grid dependence tests of the solution: local Nusselt number at $y/H = 0.5$ for the square cavity ($Ra = 1.58 \times 10^9$ and $\phi = 90°$).

ture of the temperature profiles is accurately captured by all grids at the end of the thermal boundary layer near both walls.

6. Results and discussion of the undulated cavity

One difficulty in validating the present numerical method and evaluating the turbulence model is that, to the authors' knowledge, there are no available experimental data for turbulent natural convection in undulated cavities. The parametric study of such a configuration could be employed for industrial needs such as the examples cited at the end of the conclusion. Therefore, comparison of the results obtained by low-Reynolds-number is reduced to those predicted by different grids. The grid used in this study is successively refined from 100×100, 120×120 to 160×160.

As illustrated in Fig. 8, the calculated profiles for the vertical velocity component and temperature are in satisfactory agreement, which ensures the grid independence of the solution. At the mid-width, the general trend of the presented quantities is similar to the square cavity. However, due to the undulation, the profiles are now asymmetric. The maximum value of the vertical velocity component is different at the hot wall region to the cold one in the

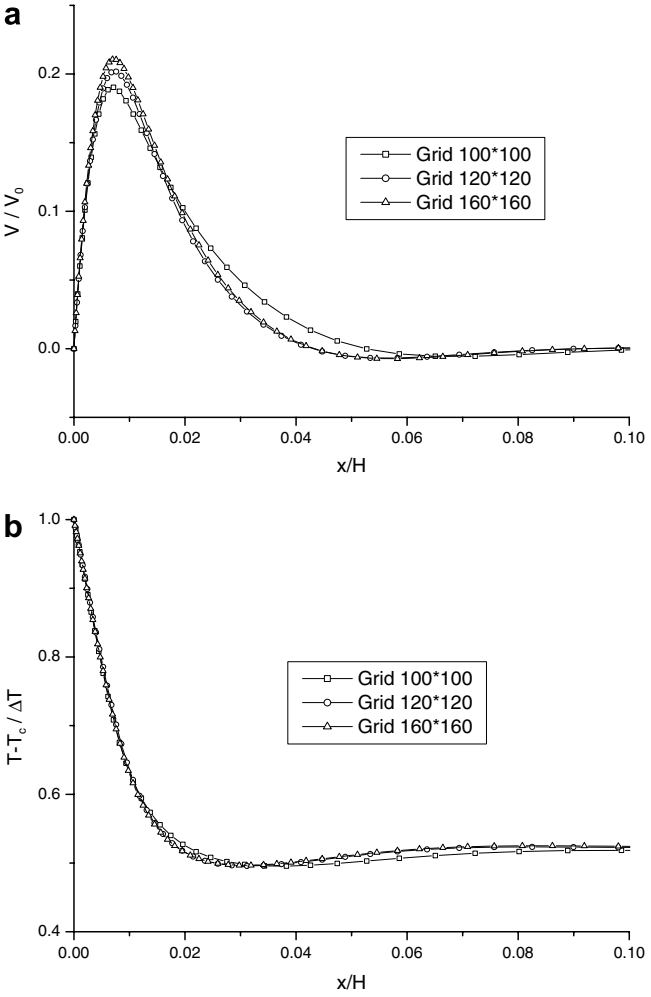

Fig. 8. Comparison of the vertical velocity (a) and the temperature (b) at $y/H = 0.5$ for the undulated cavity ($Ra = 1.58 \times 10^9$ and $\phi = 90°$).

boundary layer and falls to zero in the majority of the core of the enclosure. The turbulent flow is observed to be more accelerated near the hot wall while it is delayed near the cold wall. No discrepancy is observed between the tested grids for the vertical velocity component and the temperature. Fig. 9 shows the wavy trend of local Nusselt distribution on the wavy hot wall of the cavity due to the presence of the undulations. It may also be noticed that the local Nusselt number profile is wavy with different frequencies. Again, no noticeable different grids tested. The turbulence causes an increase in the convective heat transfer on wall surfaces. Since no appreciable difference exists between the solutions of the grids tested, the grid of 120×120 is retained for all subsequent calculations.

Fig. 10 shows the velocity vectors at the bottom colder corner and the top hot corner respectively for the configuration with an inclination angle of 90° and a Rayleigh number of 1.58×10^9. The figure shows the typical patterns observed in natural convection flows, the turbulent boundary layers on the thermally active wall. The mean temperature is nearly uniform in Fig. 11. The fluid velocity is very small and so is turbulence level, turbulence stresses and heat flux. At the angle of 90°, the gravity is parallel to the isothermal hot and cold walls. Thus, the body force exerted on the fluid is greater and the flow velocity increases yielding a stronger convection flow. At the Rayleigh number of 1.58×10^9, the rotation disturbs the flow at the corners and a centre-saddle combination is formed in both; the right upper and the left lower ones with fast counter clockwise rotating fluid as indicated in the figure. The boundary layer is developed in both vertical walls following the counter clockwise rotation. The distortion of the temperature field is due to the increase in speed of the counter clockwise rotating cell. The cold mass of fluid accelerates along the horizontal wall when suddenly exposed to the conditions of the vertical walls; it starts to move in the vertical direction. The flow predictions also reveal that the flow tends to form small secondary rolls

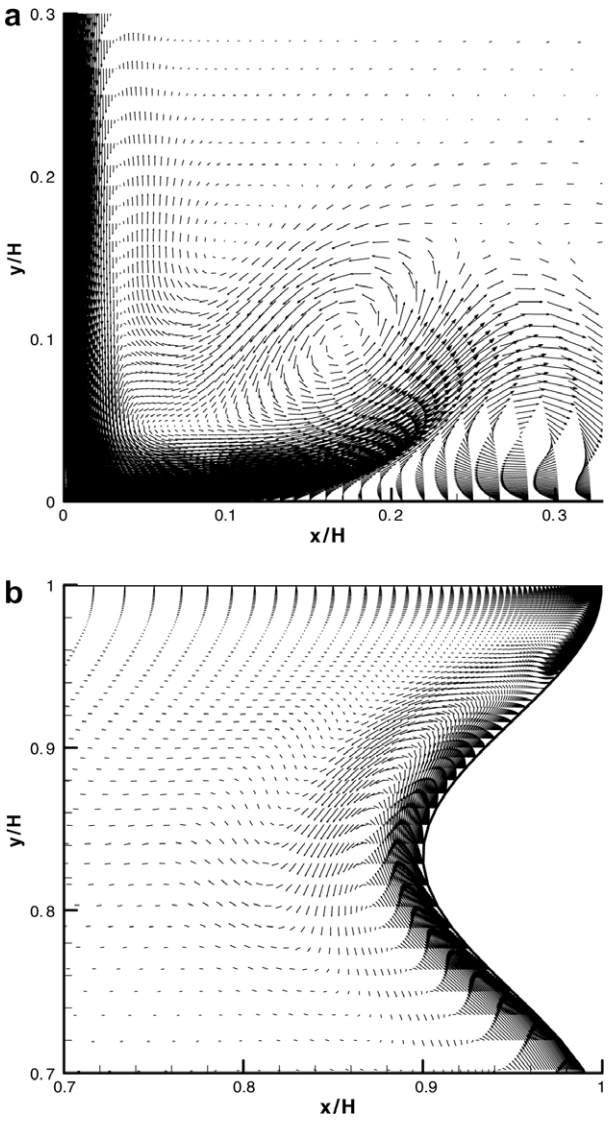

Fig. 10. Velocity vectors for the undulated cavity: (a) mean flow in the bottom colder corner; (b) mean flow in the top hot corner ($Ra = 1.58 \times 10^9$ and $\phi = 90°$).

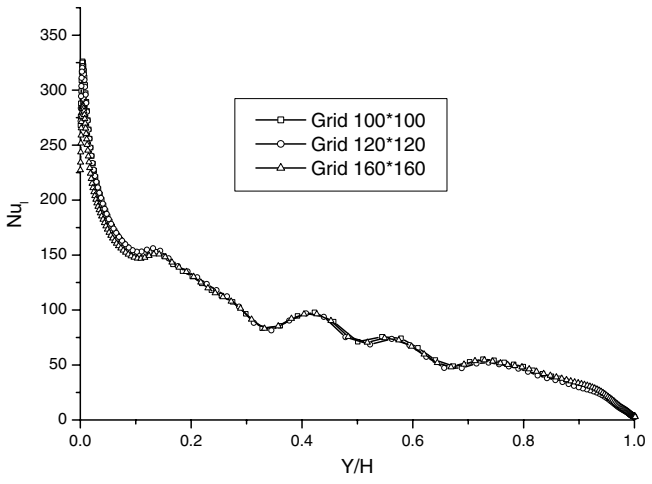

Fig. 9. Comparison of the local Nusselt number at the hot wall for the undulated cavity ($Ra = 1.58 \times 10^9$ and $\phi = 90°$).

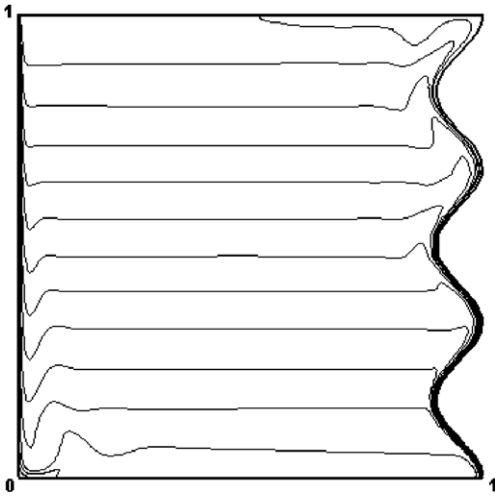

Fig. 11. Iso-temperature distributions for the undulated cavity ($Ra = 1.58 \times 10^9$ and $\phi = 90°$).

in the downstream corners of each adiabatic vertical wall. These secondary rolls and the adjacent positions of the boundary layers on the horizontal are characterised by high levels of turbulence. In addition, these rolls cause a strong variation of flow properties and local Nusselt number, i.e. conspicuous peaks of Nusselt numbers coincide with these locations.

Fig. 12 shows the comparison of the turbulent viscosity for both cavities. The profile of the turbulent kinetic energy is symmetric for the square cavity contrary to the undulated one. The turbulent kinetic energy reaches its maximum close to the walls and in the middle region. For the undulated cavity, the effect of the undulation is well established by an asymmetric profile. The turbulent kinetic energy is more consistent near the wavy wall showing high turbulence level in this region. Fig. 13 represents the comparison made between the local Nusselt number distributions for the undulated cavity and the results of the square enclosure for a Rayleigh number of 1.58×10^9 and an inclination angle of 90°. The wavy feature of the geometry undulation is well established on the local Nusselt number. Interestingly, the undulation frequency of the Nusselt distribution is different from the undulated wall frequency. As can be seen from this figure, the undulation effect increases the local Nusselt number and consequently the mean Nusselt number. In contrary to the laminar regime, the undulated wall causes an increase of the turbulent heat transfer rate.

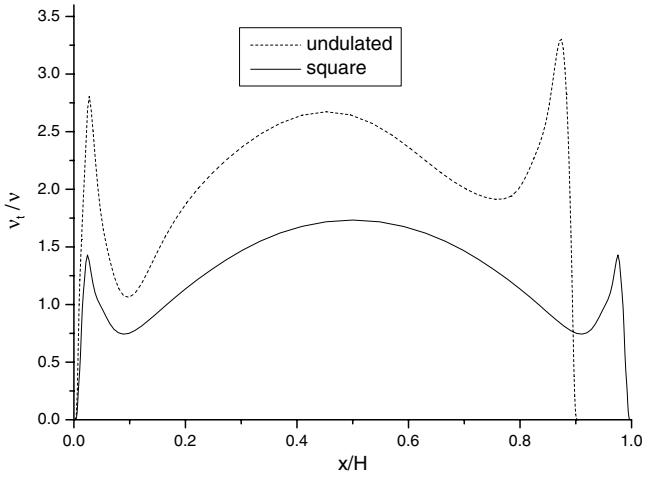

Fig. 12. Comparison of the turbulent viscosity at $y/H = 0.5$ ($Ra = 1.58 \times 10^9$ and $\phi = 90°$).

Comparison of the averaged Nusselt number as a function of the Rayleigh number between the undulated and the square cavities for an angle of 90°, is presented in Fig. 14. This comparison is made for a Rayleigh numbers up to 10^{12} (the grid independence has been also tested for this Rayleigh number). The figure shows a clear influence of the wall undulations. In comparison to the square cavity, larger values of the Nusselt number are observed. The dependency between these two numbers is presented in $\log_{10}-\log_2$ diagram. In general, the mean Nusselt number increases linearly with the increase of the Rayleigh number for both cavities. This is accord with previous findings that the Rayleigh–Nusselt relationship is linear up to $Ra = 10^{12}$. The present correlation can be applied to predict the heat transfer function of Rayleigh number. Again, the influence of the wall undulation is clearly seen in this figure by an important increase in Nusselt number in comparison to the square cavity. A correlation for the undulated cavity is proposed as follow:

$$Nu_a = 0.13Ra^{0.3} \tag{20}$$

Fig. 15 shows the averaged Nusselt number variation against the inclination angle for a Rayleigh number of 1.58×10^9 in the angle range of 90–180°. Despite the fact that the present Rayleigh number is different from the one considered by Ozoe et al. [29], the behaviour of the

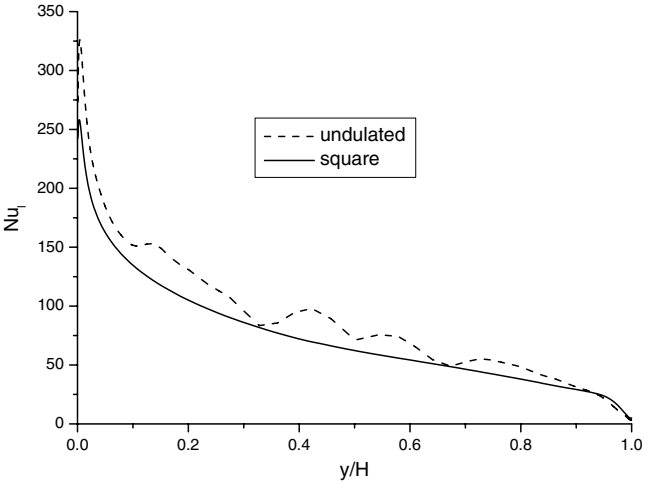

Fig. 13. Comparison of local Nusselt number results ($Ra = 1.58 \times 10^9$ and $\phi = 90°$).

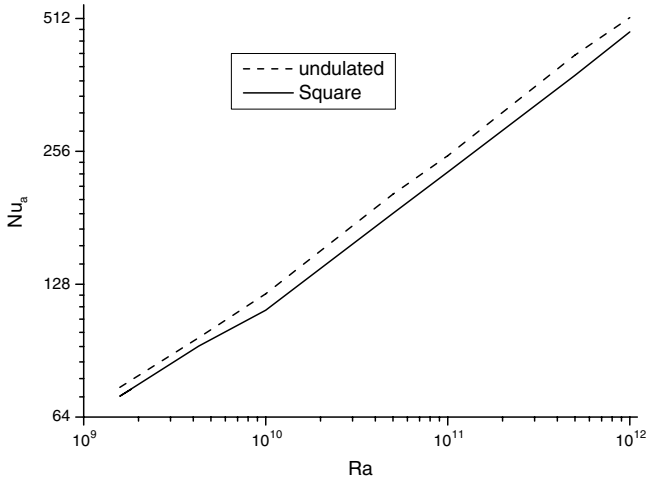

Fig. 14. Profile of the mean Nusselt number as a function of the Rayleigh number; results for the angle of $\phi = 90°$.

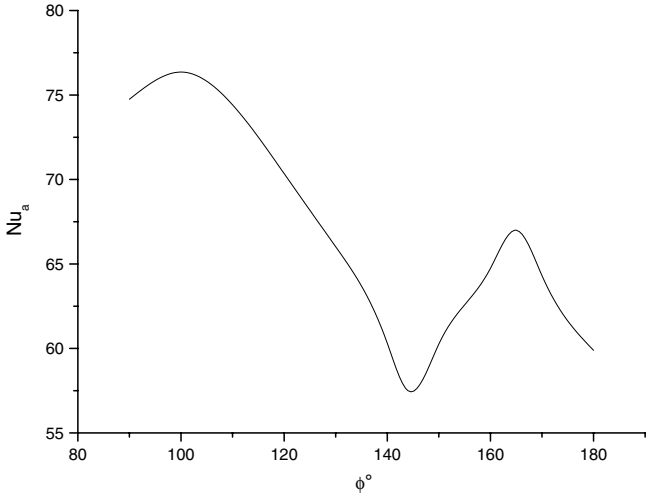

Fig. 15. Mean Nusselt number distribution as a function of the inclination angle at $Ra = 1.58 \times 10^9$.

mean Rayleigh number is still qualitatively comparable. As illustrated in the figure, the Nusselt number increases and reaches its maximum at an angle of 100°, then decreases to the minimum value of 54 when the inclination angles reaches 144°. Thus, if one is using the undulated cavity as a solar collector, it is more efficient to incline it by an angle of 144° to obtain the lower heat transfer rate. Fig. 16 shows a comparison of the turbulent kinetic energy profiles for different inclination angles. First, the turbulent kinetic energy is more significant close to the wall for all inclination angles tested. An increase of the inclination angle from 110° to 130° suddenly increases the turbulent kinetic energy in the core of the cavity. The distributions of local Nusselt number for different amplitudes with three undulations and $Ra = 1.58 \times 10^9$ are shown in Fig. 17. The same trend is observed for the tested amplitudes. There is a decrease of the local Nusselt number on the whole hot wall with an increase in the amplitude of the undulation.

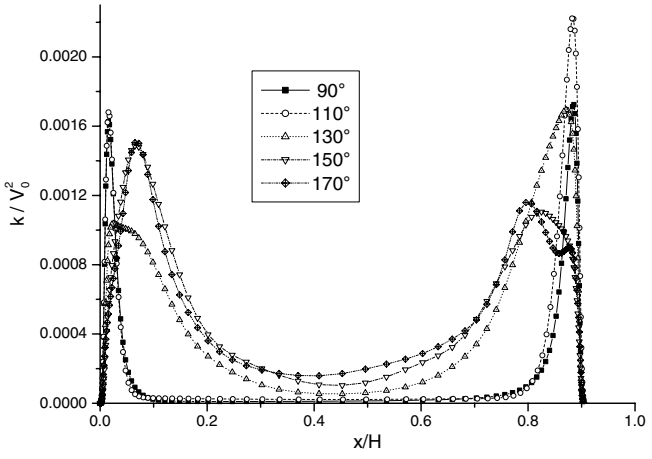

Fig. 16. Comparison of the turbulent kinetic energy at $y/H = 0.5$ for different inclination angle for the undulated cavity ($Ra = 1.58 \times 10^9$).

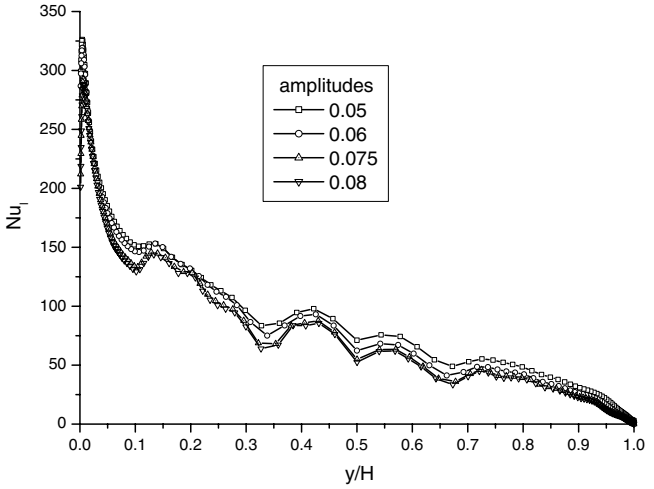

Fig. 17. Local Nusselt number distribution for the undulated cavity ($Ra = 1.58 \times 10^9$ and $\phi = 90°$).

7. Conclusion

In the present study, the effect of the undulations on the heat transfer is studied. The flow examined is of a natural convection type in a turbulent regime (Ra ranging from 1.58×10^9 to 10^{12}) with differentially heated walls. The flow is characterised by a relatively low turbulence level and thermal stratification. Two codes: FLUENT and *Code_Saturne* are used to solve the equations of mass, momentum, energy and turbulent quantities using constant properties and Boussinesq approximation for density variation. Both codes are based on the finite volume technique.

In overall, the numerical tests show satisfactory agreement with similar available data in the literature. The predictions of the RANS models in the square cavity with smooth walls revealed that the low-Reynolds k–ω–SST model returns superior results in comparison with the other RANS models. Although turbulence quantities are slightly underestimated, this model is able to reasonably reproduce the global mean flow and thermal field in satisfactory agreement with the experimental data and the coarse DNS. This gave sufficient evidence that the model is able to mimic the physical flow features in this type of geometries and was thus adopted to conduct the numerical tests of the second case with hot undulated walls.

The present study reveals that, contrary to the flow at laminar regime, the presence of the wavy wall increases the local Nusselt number. Also, the results obtained for different inclination angles and for different Rayleigh numbers are affected by the undulation of the hot wall. Indeed the latter acts on the thermal boundary layer that is thickened or thinned along this wall. Consequently, an undulation feature is visible on the local Nusselt number distribution resulting in an increase of the heat transfer rate comparing to the square cavity. The turbulence is only seen in the thin boundary layer along the vertical walls while it is totally absent in the core of the cavity where the stratification is well established. A linear relationship between the

averaged Nusselt number and Rayleigh number is also found. The optimum angle of inclination, at which the lowest mean Nusselt number occurs, is about 144°. Although, the undulated walls are shown here not beneficial in solar collector cavities, at high temperatures difference, as they increase further the heat transfer, these types of undulated walls may find it attractiveness in other applications such as the optimisation of the electronic components cooling.

Acknowledgements

The authors wish to thank the School of Mechanical, Aerospace and Civil Engineering, the University of Manchester and Electricité de France R&D, MFTT, for their collaboration in the framework of TEMPUS JEP-31131-2003.

References

[1] F. Ampofo, T.G. Karayiannis, Experimental benchmark data for turbulent natural convection in an air filled square cavity, Int. J. Heat Mass Transfer 46 (2003) 3551–3572.
[2] N.C. Markatos, K.A. Pericleous, Laminar and turbulent natural convection in an enclosed cavity, Int. J. Heat Mass Transfer 25 (1984) 755–772.
[3] R.A. Kuyper, Th.H. Van Der Meer, C.J. Hoogendoorn, Numerical study of laminar and turbulent natural convection in an inclined square cavity, Int. J. Heat Mass Transfer 26 (1993) 2899–2911.
[4] R.J.A. Janssen, R.A.W.M. Henkes, C.J. Hoogendoorn, Transition to time-periodicity of a natural-convection flow in a 3D differentially heated cavity, Int. J. Heat Mass Transfer 11 (1993) 2927–2940.
[5] S.A.M. Said, M.A. Habib, M.A.R. Khan, Turbulent natural convection flow in partitioned enclosure, Comput. Fluids 26 (1997) 563–574.
[6] T.J. Craft, A.V. Gerasimov, H. Iacovides, B.E. Launder, Progress in the generalization of wall-function treatments, Int. J. Heat Fluid Flow 23 (2002) 148–160.
[7] R.A.W.M. Henkes, F.F. Van Der Vlugt, C.J. Hoogendoorn, Natural-convection flow in a square cavity calculated with low-Reynolds-number turbulence models, Int. J. Heat Mass Transfer 34 (1991) 377–388.
[8] K.Y. Chien, Predictions of channel and boundary-layer flows with a low-Reynolds-number turbulence model, AIAA J. 20 (1982) 33–38.
[9] H.S. Dol, K. Hanjalić, Computational study of turbulent natural convection in a side-heated near-cubic enclosure at a high Rayleigh number, Int. J. Heat Mass Transfer 44 (2001) 2323–2344.
[10] S.H. Peng, L. Davidson, Computational of turbulent buoyant flows in enclosures with low-Reynolds number K–ω models, Int. J. Heat Fluid Flow 20 (1999) 172–184.
[11] K.J. Hsieh, F.S. Lien, Numerical modelling of buoyancy-driven turbulent flows in enclosures, Int. J. Heat Fluid Flow 25 (2004) 659–670.
[12] P.L. Betts, I.H. Bokhari, Experiments on turbulent natural convection in an enclosed tall cavity, Int. J. Heat Fluid Flow 21 (2000) 675–683.
[13] Y.S. Tian, T.G. Karayiannis, Low turbulence natural convection in an air filled square cavity, Part I: The thermal and fluid flow field, Int. J. Heat Mass Transfer 43 (2000) 849–866.
[14] Y.S. Tian, T.G. Karayiannis, Low turbulence natural convection in an air filled square cavity, Part II: The turbulence quantities, Int. J. Heat Mass Transfer 43 (2000) 867–884.
[15] J. Pallares, I. Cuesta, F.X. Gran, Laminar and turbulent Rayleigh–Bénard convection in a perfectly conducting cubical cavity, Int. J. Heat Fluid Flow 23 (2002) 346–358.
[16] S.H. Peng, L. Davidson, Large eddy simulation for turbulent buoyant flow in a confined cavity, Int. J. Heat Fluid Flow 23 (2001) 346–358.
[17] R. Boudjemadi, V. Maupu, D. Laurence, P. Le Quéré, Budgets of turbulent stresses and fluxes in a vertical slot natural convection flow at Rayleigh $Ra = 10^5$ and 5.4×10^5, Int. J. Heat Fluid Flow 18 (1997) 70–79.
[18] T.A.M. Versteegh, F.T.M. Nieuwstadt, Turbulent budgets of natural convection in an infinite differentially heated vertical channel, Int. J. Heat Fluid Flow 19 (1998) 135–149.
[19] H.S. Dol, K. Hanjalić, S. Kenjereš, A comparative assessment of the second-moment differential and algebraic models in turbulent natural convection, Int. J. Heat Fluid Flow 18 (1997) 4–14.
[20] S. Kenjereš, S.B. Gunarjo, K. Hanjalić, Natural convection in an air-filled cubical cavity under different angles of inclinations: a benchmark study, in: G. de Vahl Davis, E. Leonardi (Eds.), Proceedings of the ICHMT Second Int. Symp. Advances in Computational Heat Transfer, Palm Cove. Queensland, Australia, Begell House Inc., New York, 2001, pp. 1357–1364.
[21] J. Salat, S. Xin, P. Joubert, A. Sergent, F. Penot, P. Le Quéré, Experimental and numerical investigation of turbulent natural convection in a large air filled cavity, Int. J. Heat Fluid Flow 25 (2004) 824–832.
[22] F. Liu, J.X. Wen, Development and validation of an advanced turbulence model for buoyancy driven flows in enclosures, Int. J. Heat Mass Transfer 42 (1999) 3967–3981.
[23] S. Kenjereš, S.B. Gunarjo, K. Hanjalić, Contribution to elliptic relaxation modeling of turbulent natural and mixed convection, in: Int. Symp. Advanced in Computational Heat Transfer, 2004.
[24] L. Adjlout, O. Imine, A. Azzi, M. Belkadi, Laminar natural convection in an inclined cavity with a wavy wall, Int. J. Heat Mass Transfer 45 (2002) 2141–2152.
[25] F.R. Menter, Two-equation eddy-viscosity turbulence models for engineering applications, AIAA J. 32 (8) (1994) 1598–1605.
[26] S. Benhamadouche, K. Mahesh, G. Constantinescu, Collocated Finite Volume Schemes for L.E.S. on Unstructured Meshes, CTR, Proceeding of the 2002 Summer Program Stanford.
[27] S. Benhamadouche, D. Laurence, LES, coarse LES, and transient RANS comparisons on the flow across a tube bundle, Int. J. Heat Fluid Flow 24 (2003) 470–479.
[28] A.G. Hutton, R.M. Ashworth, The challenge of turbulence modelling in modern aeronautical design, J. Numer. Meth. Fluids (2000) 1–6.
[29] H. Ozoe, H. Sayama, S.W. Churchill, Natural convection in an inclined square channel, Int. J. Heat Mass Transfer 17 (1974) 1209–1217.